Direct Chemical Mapping of Electrochemically Generated Spatial Composition Gradients on Thin Gold Films with Surface-Enhanced Raman Spectroscopy

Karin M. Balss, Tzu-Chi Kuo, and Paul W. Bohn*

Department of Chemistry, Beckman Institute for Advanced Science and Technology and Materials Research Laboratory, 600 South Mathews Avenue, Urbana, Illinois 61801

Received: August 14, 2002; In Final Form: October 24, 2002

Surface-enhanced Raman spectroscopy (SERS) was employed to map the composition of electrochemically generated gradients in aromatic thiols on Au electrodes. Two commonly used substrates, electrochemically roughened (ORC) and metal film over nanosphere (MFON) electrodes, were tested for this purpose. Only the MFON substrates displayed the requisite electrical continuity and signal-enhancement properties needed for vibrational spectroscopic mapping of electrochemical gradients. One-component gradients and counterpropagating two-component gradients were formed from naphthalenethiol (NPT), chlorobenzenemethanethiol (ClBMT) and acetamidothiophenol (ACT) and were characterized by Raman scattering on Au MFON substrates. The surface coverage observed approximated the coverage predicted by the combination of a linear potential gradient with local Nernstian behavior of the reductive desorption reaction. For two-component gradients of NPT/ClBMT and NPT/ACT it was possible to perform measurements of surface composition as a function of spatial position (potential), thereby achieving chemical mapping of the surface with the spatial resolution of the focused laser. Because the desorption kinetics for aromatic thiols are relatively slow, surface coverages could also be controlled by changing the length of time the electrochemical potential gradient was applied.

Introduction

Self-assembled monolayers (SAMs) of organothiols constitute a powerful system to study adsorption, wettability, adhesion, and electron-transfer mechanisms, and the ability to control the location of SAM components on metal and metal oxide surfaces is an important adjunct capability for applications in molecular recognition and controlling transport. The patterning of SAMs of organothiols can be achieved by a variety of techniques including lithography, micromachining, diffusion-reaction methods, mixing of binary components, and cross mixing in microfluidic channels.[1−5] More recently, scanning tunneling microscopy (STM) based lithography has also been used to place and remove organothiols selectively.[6] These methods, however, all suffer the drawback that the surface compositional patterns, once created, are either fixed or difficult to change.

A technique developed recently in this laboratory generates laterally varying surface compositions, which can be controlled in space and time, by mapping electrochemical reactions onto surfaces that display a lateral gradient in electrochemical potential.[7−10] An approximately linear potential gradient is created by connecting two working electrodes to opposite ends of a thin (30 nm $\leq d \leq$ 50 nm) rectangular Au strip, creating an electrochemical potential gradient depending on injected current, i, resistivity of the film, ρ, film cross sectional area, A, and V_0 the offset potential according to

$$V(x) = V_0 + \int \frac{i\rho(l)}{A}\,\mathrm{d}l \qquad (1)$$

Because the driving force for a given electron transfer reaction to occur depends on the standard potential and any relevant overpotential, and because each spatial location is characterized by a unique potential, electrochemistry occurs in a spatially dependent manner. As one example, spatial patterns of organothiols can be generated by choosing the potential gradient to encompass the adsorption/desorption potentials of organothiols in alkaline solutions (ca. −1.0 V to −0.5 V vs Ag/AgCl, depending on the specific thiol). Thiols adsorb at locations corresponding to potentials positive of the oxidative adsorption potential (∼−0.6V vs Ag/AgCl) and are stripped at potentials negative of the reductive desorption potential, resulting in a laterally varying distribution in surface coverage with saturation coverage, Γ_{sat}, on one end and zero coverage on the other. Counterpropagating two component gradients can also be created by breaking electrical contact and immersing the sample briefly in a solution containing a second thiol component, which then fills in the bare regions of the Au surface. Other electrochemical reactions can also be localized or patterned utilizing the same principle, including overpotential deposition of Cu onto Au, evolution of O_2 by H_2O_2 oxidation,[8] and Pt deposition onto indium tin oxide.[11]

Electrochemically generated gradient compositions have been visualized by spatially dependent contact angle measurements, pulsed-force mode atomic force microscopy (PFM-AFM),[10] surface plasmon reflectometry imaging,[7] X-ray photoelectron spectroscopy imaging,[8] and fluorescence imaging.[9] These imaging methods display surface coverages for one- and two-component systems consistent with those predicted by a Nernstian relationship between overpotential, $\eta(E - E^{\circ\prime})$, and surface coverage, θ,

$$\eta = \frac{2.3RT}{nF}\log\frac{\theta}{1-\theta} \qquad (2)$$

yielding surface coverage vs potential (or equivalently, position) plots, which are sigmoidal with a half-width of 60 mV. However, they measure largely physical properties as a function of spatial position. Direct chemical mapping, for example using

10.1021/jp021875y CCC: $25.00
Published on Web 01/07/2003

the variation in terminal functional group composition as a function of position, has not been performed to date. Vibrational spectroscopy is the natural choice for direct chemical mapping of these distributions. External reflection Fourier transform infrared spectroscopy (FTIR) has been employed to study surface coverage and order in SAMs[12−14] and gradients prepared by diffusion methods have also been mapped.[5] However, the infrared approaches capable of high sensitivity monitoring of submonolayer surface coverages are not compatible with high spatial resolution, because they principally rely on large angles of incidence.

The aromatic thiols are an especially interesting class of SAMs. They have been examined for their potential use in molecular electronic and optoelectronic devices.[15,16] It has also been shown that arenethiols are more effective at preventing oxidation of thiols to thiolates compared to straight chain counterparts.[17] The self-assembly of aromatic systems has been studied with a variety of techniques, including contact angle measurements, ellipsometry, FTIR reflection spectroscopy, surface-enhanced Raman spectroscopy, electrochemistry, and scanning tunneling microscopy (STM).[17−23] Depending on the structure of the aromatic thiol, well-ordered monolayers can be formed, especially for those in which a methylene spacer is placed between the sulfur headgroup and the aromatic moiety.

In the present experiments surface-enhanced Raman spectroscopy (SERS) is employed to examine the surface coverage and structure of one- and two-component aromatic thiol gradients on Au electrodes for several reasons. In situ measurements are possible with Raman spectroscopy, but difficult in IR, due to the interference from H_2O. In addition, with an appropriate substrate, surface-enhanced Raman spectroscopy (SERS) can provide signal enhancement factors of 10^4-10^6, sufficient to examine submonolayer coverages. Furthermore, with appropriate optics, it is possible to image samples with micrometer scale resolution.[24] The combination of high spatial resolution and submonolayer detection limits is not achievable by infrared spectroscopy.

A variety of SERS substrates have been used to study SAMs, including metal island films on glass,[25,26] oxidized aluminum foil,[27] and CaF_2 windows,[28] immobilized colloidal particles,[29−32] electrochemically roughened substrates produced by oxidation−reduction cycling (ORC) films,[17,33−36] and metal films over nanospheres (MFON).[37] With the exception of island films and colloidal surfaces, the above substrates are electrically continuous, and electrochemical studies can thus be performed. In situ electrochemical SERS measurements have been performed to measure free energies of adsorption, ΔG_{ads}, of alkanethiols and thermodynamic parameters of electrodeposition,[38,39] as well as conformational changes associated with applied electrochemical potential.[34,40] When electrochemically generated gradients in surface coverage are studied by Raman scattering, however, the substrate must (a) possess the properties necessary for surface enhancement and (b) be electrically continuous and sufficiently robust to withstand milliampere in-plane current injection. In this paper, we present SERS mapping of one- and two-component gradients in aromatic thiol surface coverage on MFON substrates, which were the only substrates found to meet both criteria.

Experimental Section

Materials. Absolute ethanol (EtOH) was purchased from Aaper Alcohol and Chemical Co. Optima grade methanol (MeOH) and KOH were purchased from Fisher Scientific. 4-Chlorobenzenemethanethiol (ClBMT), 2-naphthalenethiol (NPT), and 4-acetamidothiophenol (ACT) were purchased from Aldrich and used without further purification. Polystyrene beads were purchased from Sigma Aldrich and diluted in EtOH before use.

Substrate Preparation. Three types of SERS substrates were used. In each case microscope slides cut into 10 mm × 15 mm pieces were cleaned in hot piranha (4:1 H_2SO_4/H_2O_2) cleaning solution for 1 h. The samples were rinsed with copious amounts of deionized (18.2 MΩ cm) H_2O, followed by 2-propanol and dried with N_2. The samples were transferred to the evaporation chamber immediately after cleaning to minimize contamination. The base pressure during deposition was 1×10^{-6} Torr. The first substrate was a Au island film prepared by depositing a 63 Å mass thickness onto the glass. The second substrate to be used as an Au ORC film was prepared by depositing chromium (1 nm) to promote adhesion followed by 50 nm of Au. These films were then subjected to a cleaning step by cycling five times from −0.2 to +1.2 V in 1 M H_2SO_4(aq) at 100 mV/s, followed by 0−20 consecutive oxidation−reduction cycles[17,33−36] in 0.1 M KCl(aq) at 500 mV/s. The third substrate was the MFON substrate. After the initial gold deposition was performed (1 nm Cr and 30 nm Au), the samples were removed from the evaporation chamber. A solution containing either polystyrene or silica nanospheres with diameters in the range 50 nm ≤ d ≤ 450 nm in EtOH/H_2O was spin coated onto the substrates (3400 rpm for 20 s). The samples were then transferred back to the deposition chamber, and an additional 200 nm of Au was then deposited.

Electrochemistry. The stripping of aromatic thiols was examined on thermally deposited gold films on glass microscope slides and MFON substrates. Cyclic voltammograms were collected with a bipotentiostat (Pine Instruments, Model AFCBP1) in 0.5 M KOH/MeOH electrolyte purged with Ar for 15 min. Voltammograms were acquired at 100 mV/s between −0.3 and −1.3 V vs Ag/AgCl. The active area of the electrode was 0.187 cm^2.

Gradient Preparation. Au films were immersed in 1 mM ethanolic thiol solutions for 12 h to assemble the first component. A bipotentiostat, employing a saturated Ag/AgCl reference electrode and a Pt counter electrode in deaerated 0.5 M KOH/MeOH, applied the desired electrochemical potentials to the two ends of the working electrode to prepare the gradients. Contacts to the electrode surface were made by Au wires pressed onto the film in a Kel-F cell. Typically, alkanethiol/Au SAMs were electrolyzed with 70 mV mm^{-1} in-plane potential drops for 30 min. The stripping potential was located approximately in the center of the film by setting the potential ranges to −300 to −1300 mV vs Ag/AgCl at the extreme ends. Two-component gradient samples were first checked by acquiring Raman spectra of the one-component precursor gradient. The samples were then reimmersed in a second thiol solution for time periods of 30 s to 2 min. Gradients composed of NPT/ClBMT and NPT/ACT were prepared in this manner. The first component listed in all cases refers to the first thiol assembled.

Raman Spectroscopy. Raman spectra were obtained with a Spex 500M single monochromator equipped with a 600 groove/mm grating and Photometrics CCD camera. The excitation was 752.5 nm from an Ar^+-laser pumped Ti−sapphire laser. A holographic band rejection filter (Kaiser Optical Systems Inc.) was used to diminish the Rayleigh scatter introduced into the spectrometer. The optical train consisted of a cylindrical lens to focus the excitation beam to a line (≈100 μm × 0.5 cm) on the sample at an incident angle of 55° for ex situ and 40° for in situ measurements. The laser power was typically 150−200

mW. Spectra on MFON substrates were typically acquired with 1−2 min integration times averaged over 30 min. The samples were mounted on a micrometer stage, and spectra were typically collected in 2 mm increments. The band assignments were based on literature assignments as well as molecular simulations with Cerius2 (Accelrys, Inc.) and Gaussian 98 (Gaussian Inc.) using density functional theory B3LYP with 6-31G(d) basis.[17,22] The bands were fit to a Voigt function and baseline corrected for intensity measurements. In situ measurements were made with a spectroelectrochemical flow cell made out of black Kel-F. The counter electrode and reference electrodes were Au and Ag wire, respectively. A fused silica plate was used as the optical window. To test signal reversibility, the film was subjected to the following cycle: (a) 45 min assembly in 1 mM ethanolic thiol solution, (b) rinsing with ethanol and water, (c) collecting spectra at open circuit in 0.1 M KCl_{aq}, (d) collecting spectra at −1 V for 30 min, and (e) rinsing with water and then ethanol. The spectra were collected from the same physical location in each case. Adsorption behavior was also measured with this cell by subjecting the film to the following cycle: (a) assembly in thiol solution (three different concentrations spanning 4 orders of magnitude) as a function of time, *t*, (b) rinse with ethanol and water, (c) collect spectra in 0.1 M KCl, (d) rinse with water and ethanol.

Atomic Force Microscopy. AFM measurements were performed with a Digital Instruments Multimode AFM Nanoscope III instrument in tapping mode. Typical scan rates of 0.5 Hz and 512 samples/line were obtained. Three-dimensional rendering was performed with Maya (Alias/Wave front) software.

Results and Discussion

Substrate Characterization. The objective of these experiments is to map the distribution of terminal functional moieties produced in electrochemically generated gradients. To be suitable for these experiments, the substrate must simultaneously be capable of (a) supporting a linear gradient in electrochemical potential when subjected to milliampere current injections and (b) providing the necessary SERS enhancement. Two classes of SERS electrodes were tested for this purpose, Au ORC and MFON substrates. Au island films were also tried initially, but it proved impossible to obtain films reliably that could both provide strong SERS enhancement and maintain electrical continuity. Substrate roughness was characterized both by AFM and electrochemical measurements.

AFM measurements in Figure 1 show a typical MFON substrate, revealing that these MFON substrates have substantially less than monolayer nanosphere coverage. Under preparation conditions employed here coverage ranged between 0.16 and 0.21 monolayer. The high-resolution topography image, Figure 1b, shows the Au deposited on top of the beads. Step edges and roughness features are visible in this image. The rms roughness was also measured on Au ORC substrates as a function of ORC cycles. The rms roughness ranged from 2 nm on the unprocessed substrates to 12 nm for 20 ORC cycles. After 20 cycles, the ORC films became discontinuous and could no longer be used for gradient preparation.

Confirmation of thiol assembly and proper electrochemical behavior on MFON and ORC substrates was tested by comparing the stripping potential of the aromatic thiols on thermally evaporated Au substrates to that on ORC and MFON Au electrodes. In general, the stripping peak observed on MFON and ORC substrates was broader than that on thermally evaporated Au. Two peaks were observed for NPT desorption, as has been observed previously for desorption from polycrystalline Au.[21] On thermally evaporated Au films a large desorption peak was observed at −0.69 V with a smaller wave appearing at −0.91 V vs Ag/AgCl. The desorption from MFON substrates occurred at −0.89 and −1.20 V with comparable relative sizes. These compare to desorption potentials reported in aqueous KOH for NPT on Au on mica of −0.65 and −1.04 V vs Ag/AgCl.[21]

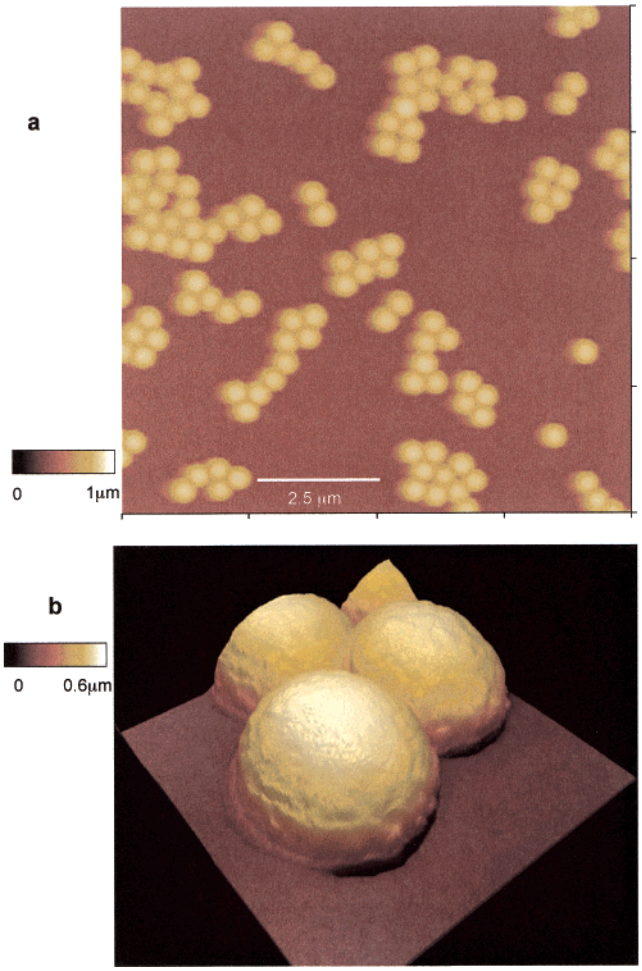

Figure 1. (a) 10 μm × 10 μm AFM topography map of a typical MFON substrate, showing the submonolayer bead coverage. The lateral 2.5 μm scale bar indicates scaling for the two in-plane dimensions. In both images the color scale indicates height according to the scale bar at the left. (b) 1 μm × 1 μm topography image rendered in 3-D.

The surface coverage of NPT can be estimated from the integrated charge of the reductive desorption peak. These measurements rely on knowing the geometric area of the electrode corrected by a surface-specific roughness factor. Roughness factors have been estimated to be 1.2 from STM cross sections for Au (111) on mica.[41] Surface roughness factors have also been calculated from gold oxide formation and removal in H_2SO_4.[42] If roughness factors of 1.2 and 3 are used for planar and MFON electrodes, respectively, the coverages are 5.4×10^{-10} and 7.4×10^{-10} mol cm^{-2}, which compare well to the reported coverage for NPT on gold foil electrodes of 7.1×10^{-10} mol cm^{-2}.[21] The measured desorption potential of ClBMT (−0.84 V vs Ag/AgCl) was also in good agreement with literature values.[19] The electrochemical performance of Ag and Au MFON electrodes has been investigated by Van Duyne and co-workers with a reversible redox couple and found to exhibit ideal behavior up to scan rates of 250 mV/s.[37] Similar behavior was observed with our MFON electrodes. The ΔE_p values for an $Fe(CN)_6^{3-/4-}$ couple measured on planar Au and MFON substrates were the same to within 10 mV.

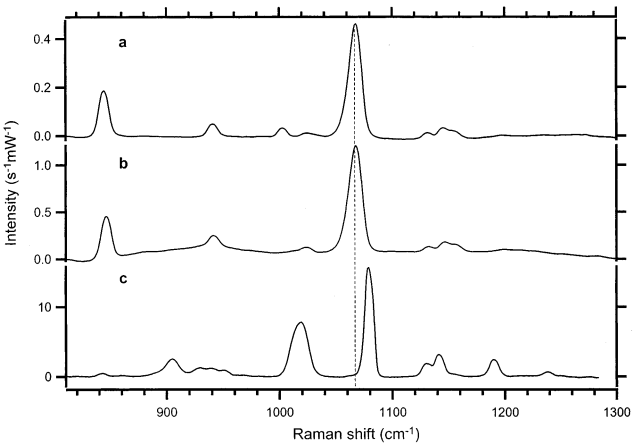

Figure 2. Comparison of Raman spectra from 2-naphthalenethiol (NPT) on (a) MFON electrode, (b) Au island film, and (c) neat (solid). Note that the *y*-axis scale varies for each spectrum.

A key question for these studies is whether the nanospheres used to generate SERS enhancement on MFON substrates perturb the potential gradient. According to eq 1, the potential should vary in a linear fashion. However, the resistivity of the film has contributions from the local surface morphology as well as molecular adsorbates according to

$$V(x) = V_0 + \int \frac{i\rho(l)}{A}\,\mathrm{d}l + \delta(x) + \kappa\Gamma(x) \qquad (3)$$

where $\delta(x)$ is a position dependent variation associated with surface morphology, $\Gamma(x)$ is the adsorbate surface density, and κ is an adsorption-dependent sensitivity factor. Previous work from this laboratory has shown that the second and third terms contribute at most 5% of the spatially dependent potential in Au-organothiol systems.[43−45] Furthermore, the diameter of an individual nanospheres (450 nm) used in these experiments would constitute 32 mV (0.003% full scale) in potential space on the substrate. Although nonlinear variations in the local potential are clearly possible, the density of beads and their size ensure that any variations are small compared to the overall potential gradient. Of course, the ultimate test of this approximation is in the measured composition profiles and their relation to predicted profiles.

Comparison of Substrates and Monolayer Characterization. SERS spectra were collected for a variety of aromatic thiols on both ORC and MFON substrates with the objective of finding suitable bands for use in mapping one- and two-component gradients. The Au ORC substrates displayed small, i.e., 10× less than comparable MFON substrates, signals that were nonuniform across the film. Irreversible loss of SERS signal was also observed for ORC films after exposure to negative potentials, as reported by others.[37] For all of these reasons the bulk of the work presented here focuses on Au MFON substrates.

To be useful in chemical mapping it is important that thiols possess a unique Raman band that scales linearly with surface coverage. Thus, SERS spectra from MFON and Au island films were collected for several candidate aromatic thiols and compared to the corresponding neat Raman spectrum. Figure 2 compares spectra of NPT on a MFON substrate, a Au island film, and neat, whereas Figures 3 and 4 do the same for ClBMT and ACT, respectively. The island film substrates served as a convenient standard SERS substrate for initial thiol characterization, even though they cannot be used to prepare electrochemical gradients. The bands of interest appear in the region 800−1300 cm^{-1}. Most of the bands in this region are attributed to the

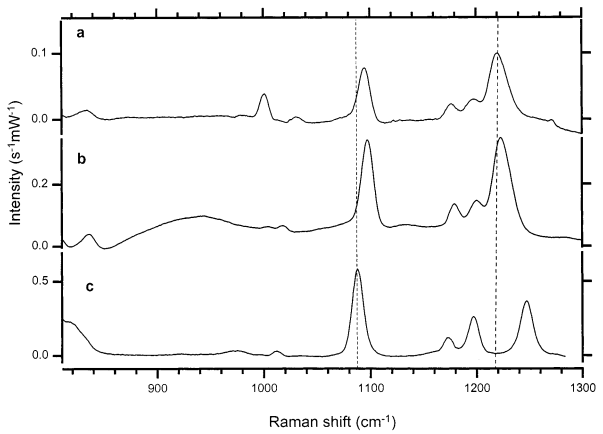

Figure 3. Comparison of parachlorobenzenemethanethiol (ClBMT) on (a) MFON electrode, (b) Au island film, and (c) neat (liquid). Note that the *y*-axis scale varies for each spectrum.

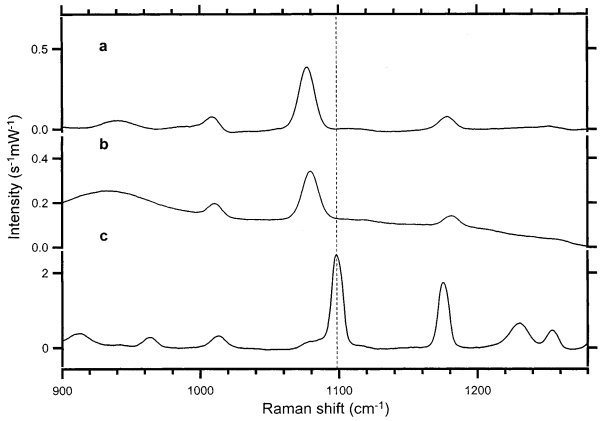

Figure 4. Comparison of 4-acetamidothiophenol (ACT) on (a) MFON electrode, (b) Au island film, and (c) neat (liquid). Note that the *y*-axis scale varies for each spectrum.

aromatic moiety with the exception of a CH_2 wag at 1221 cm^{-1} observed in ClBMT. The Raman shifts on island films and MFON substrates were very similar with differences <5 cm^{-1} in all cases. The 1068 cm^{-1} band (in plane symmetric bending of ring attached to S) and 844 cm^{-1} band (CH out-of-plane bend or ring deformation)[46] on the MFON substrates are unique to NPT, Figure 2. The 1068 cm^{-1} band in the surface spectra is downshifted ∼12 cm^{-1} from the neat spectrum, and the 844 cm^{-1} band is enhanced relative to other peaks on the SERS-active substrates. The observed downshift and enhancement of these bands can be correlated with the orientation of NPT and in particular the naphthyl moiety. Electrochemical stripping analysis indicates a coverage (7.4×10^{-10} cm^{-2}) that is much greater than that calculated for NPT with the naphthyl ring oriented parallel to the surface (4.0×10^{-10} mol cm^{-2}). In addition, SPR thickness calculations agree with coverages consistent with a ring orientation perpendicular to the surface. Evidence for chemisorption is found in the SH bending (905 cm^{-1}) and SH stretching (∼2560 cm^{-1}) bands, both of which disappear in the SERS spectra, indicating disruption of the S−H bond upon self-assembly onto the Au surface.

Bands unique to ClBMT are observed at 1221 cm^{-1} (CH_2 wag) and 1095 cm^{-1} (in plane symmetric bend); viz. Figure 3. The 1221 cm^{-1} band is downshifted 26 cm^{-1} in the surface spectra, whereas the 1095 cm^{-1} band, assigned to an in-plane ring vibration, is shifted 7 cm^{-1} to higher frequency in comparison to neat ClBMT. The position and intensity of the 1221 cm^{-1} band are in good agreement with results observed by Garrell and co-workers[22] for ClBMT on ORC substrates in

KCl. The 1095 cm^{-1} band, however, is shifted in the opposite direction to that observed on ORC substrates and to the similarly positioned band in NPT. Because there is an extra methylene between the S headgroup and the aromatic moiety in ClBMT compared to NPT, it is reasonable to posit a different orientation for the aromatic ring relative to the local surface plane as a reason for the opposite shift of the in-plane ring vibration. Monolayers of ACT were also characterized on island and MFON substrates, Figure 4. The unique band of interest in ACT (1080 cm^{-1}) is again downshifted ~20 cm^{-1} from the neat spectrum and is assigned to an in-plane symmetric bend. Just as in NPT, the S headgroup is bonded directly to the aryl ring, and the in-plane symmetric ring mode is downshifted in the surface spectrum.

In addition to these spectra of one-component films, gradients were prepared from NPT/ClBMT and NPT/ACT. Spectral peaks characteristic of a single component were easily resolved in gradients prepared from NPT and ClBMT, whereas gradients prepared from NPT/ACT required peak fitting to separate the individual components. Adsorption behavior was characterized by following shifts in the surface plasmon resonance (SPR) response and comparing to adsorption information obtained in situ by SERS. The integrated areas of the unique bands in the SERS spectra are proportional to the surface coverage calculated from SPR data indicating that, under these conditions, the SERS band intensities can be used to estimate surface coverage when mapping one and two-component gradients.

Stability of SERS Signal. Because gradients of aromatic thiols were routinely exposed to extreme negative potentials (−1.3 V vs Ag/AgCl) for time periods up to 30 min, and because the ORC substrates had been shown to suffer irreversible loss of SERS activity at negative potentials, the stability of the SERS signal from MFON substrates was investigated upon exposing the film to electrochemical potential gradients. Using the in situ cell, SERS spectra of full monolayers of either NPT or ACT were collected at open circuit in 0.1 M KCl(aq), after which the films were subjected to gradient-forming potential programs. Then the gradients were stripped, a new SAM was formed, and SERS spectra of the resulting monolayers were then collected. Although signal intensities were found to change after each cycle, the signal was not degraded irreversibly. Changes in intensity from cycle to cycle could be attributed to a different saturation coverages achieved during each assembly or by morphological variations induced by application of negative potentials. Because one-component gradients are prepared by stripping a portion of the monolayer film, SERS intensities are always referenced to signals from the full coverage portion of the sample, i.e. the portion of the sample that is not exposed to negative potentials. Thus, changes in intensity that affect the entire sample do not pose a problem in interpretation, thereby illustrating the feasibility of using MFON substrates for preparing and mapping electrochemically generated gradients.

SERS of One-Component Gradients. The composition as a function of position was investigated with one-component gradients composed of NPT and ClBMT. Figure 5 shows a series of spectra as a function of position along a 14 mm NPT gradient prepared with a 64 mV mm^{-1} in-plane gradient. The trace at −1 mm (top spectrum) is the NPT monolayer prior to electrolysis. The variability in signal as a function of position on a single substrate (before electrolysis) was low, with an average of the integrated area of the 1068 cm^{-1} mode of 9.8 ($\pm$0.1) $\times$ 10^4 (average $\pm$ one standard deviation from three locations on the film). Figure 6 is a plot of the surface coverage as a function of position (potential) along the film. Clearly the composition varies spatially as expected from the applied

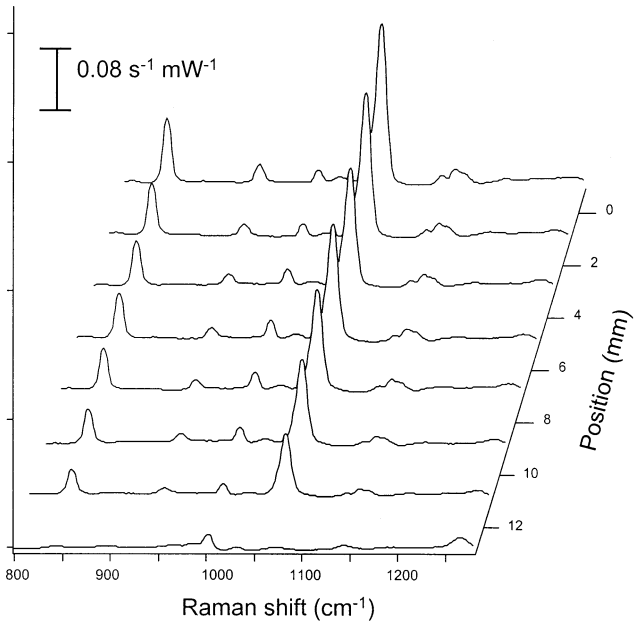

Figure 5. SERS spectra from a one-component gradient of NPT on a 14 mm film (30 min electrolysis at 64 mV mm^{-1}). The right *y*-axis is position in millimeters. The spectrum at −1 mm represents an average of three monolayer spectra collected at three spots on the sample before electrolysis. Spectra were collected by averaging 20 integration periods of 1 min at 140 mW.

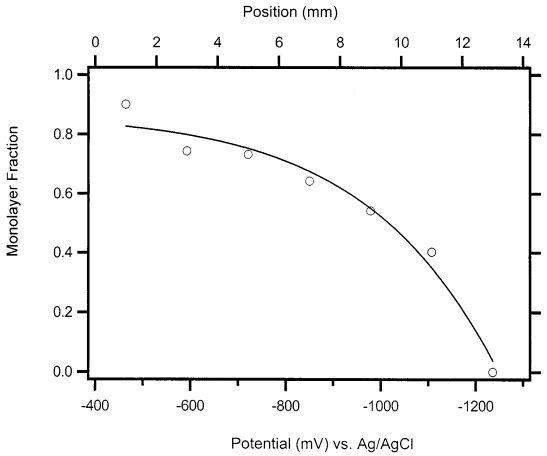

Figure 6. NPT surface coverage as a function of spatial position for the gradient presented in Figure 5. Surface coverages were inferred from the integrated area of the 1068 cm^{-1} band and calibrated against quantitative coverages measured by SPR. The solid line is a fit to eq 4.

electrochemical potential gradient. After 30 min of electrolysis, the film on the adsorptive end (1 mm) of the film had >90% monolayer coverage, but the film retained <1% of the original NPT on the desorptive end (13 mm). The solid line in the figure gives a fit to a sigmoidal function of the form

$$I(x) = I_b + \frac{I_m}{1 + e^{(x_0 - x)/r}} \qquad (4)$$

where I_b is the base value, I_m is the normalized maximum value, x_0 is the inflection point, and r is a spatial rate constant related to the slope in the transition region.

One-component gradients were also prepared from NPT and ClBMT with short and intermediate electrolysis times (<2 min and <15 min). Shorter electrolysis times yielded films with 100% coverage on the adsorptive (positive) end, decreasing

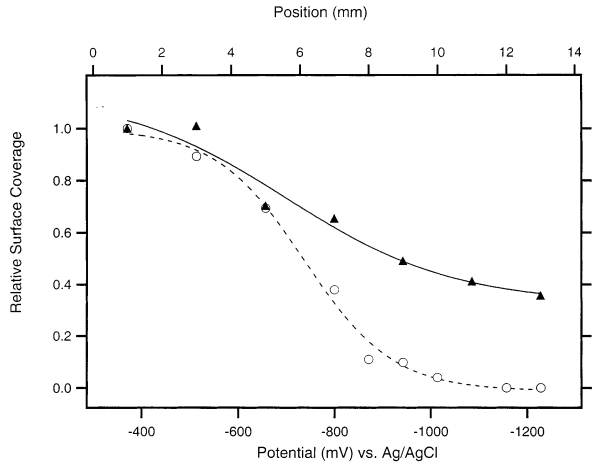

Figure 7. NPT surface coverage as a function of spatial position for one-component gradients of NPT prepared with 15 min (▲) and 30 min (○) gradient applications. Surface coverages were inferred from the integrated area of the 1068 cm^{-1} band and calibrated against quantitative coverages measured by SPR. The lines are fits to eq 4.

surface coverage along the film and incomplete depletion (<60% coverage) on the stripping (negative) end of the film. Previous work with straight chain alkanethiol systems revealed that even short electrolysis times were sufficient to achieve surface coverages that approached zero on the desorptive end of the film.[7−9] The observed difference in desorption kinetics could result from inherent differences in the electron-transfer rates between straight chain and aromatic thiol systems or morphological effects on electrode kinetics. To assess these two possibilities the desorption of aromatic thiols from MFON substrates was monitored in situ with the spectroelectrochemical cell. At positions corresponding to potentials negative of the desorption potential, surface coverage decayed exponentially in time, with coverages approaching zero at times greater than 20 min. Because the desorption rate for aromatic thiols is slow at modest overpotentials, the rate of desorption affords another experimental control on the surface composition at a given spatial location. Figure 7 compares surface coverage maps for two one-component gradients prepared with 15 and 30 min gradient application times, respectively. Clearly, both samples show the gradient in surface coverage with the sample subjected to a shorter stripping time having a noticeably larger Γ_{NPT} at the negative end of the electrode.

SERS of Two-Component Gradients. In many applications it is desirable to have two disparate functional groups in counterpropagating gradients, so that some physical property, e.g., wettability, may be laterally varied in a controlled fashion. Thus, two-component gradients were prepared and the composition mapped as a function of position, or equivalently, potential. The two-component gradients were prepared by starting from the one-component gradient samples, so that the surface coverage relative to that of the first component could be measured. Several combinations of aromatic thiol were used. NPT/ClBMT was chosen because the modes identifying each component are well resolved. Figure 8 shows the SERS spectra acquired at varying locations on the NPT/ClBMT gradient. This sample was prepared by starting with a one-component NPT gradient, which had been stripped for 15 min, so that removal of NPT from the negative end of the gradient was incomplete. This one-component gradient was then immersed in ClBMT solution for 1 min. Measurements on the one-component gradient showed that less than 36% original coverage of NPT remained on the negative end of the gradient (position 13 mm) after electrolysis. The spectra show that both components can

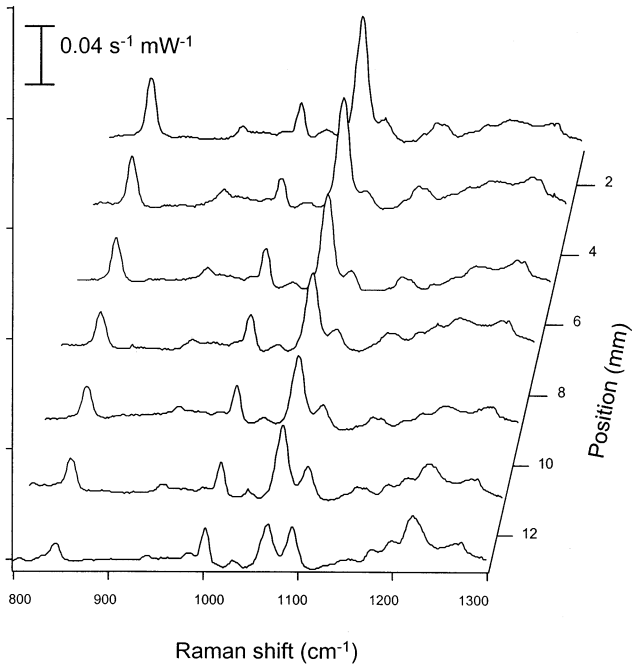

Figure 8. SERS spectra of NPT/ClBMT two-component gradient as a function of position (potential). From position 13 mm to 1 mm, ClBMT intensity decreases and NPT increases. Spectra were collected by averaging 15 integration periods of 2 min at 200 mW.

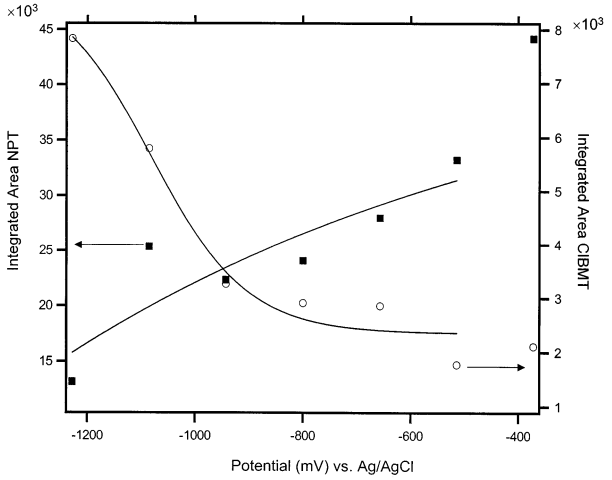

Figure 9. Integrated areas of the 1068 cm^{-1} (NPT) and 1095 cm^{-1} (ClBMT) bands as a function of position (potential) for an NPT/ClBMT two-component gradient. The solid lines are fits to eq 4.

be observed at the two extreme ends of the gradient although with intensities characteristic of the local concentration. Figure 9 is a plot of the integrated area of the unique bands (1068 cm^{-1} of NPT and 1095 cm^{-1} of ClBMT) as a function of position and potential along the film. These areas can be used to calculate the surface coverage. The original NPT gradient exhibited 0.36 monolayer NPT on the negative end, which then decreased to 0.30 monolayer NPT after formation of the NPT/ClBMT two-component gradient. Repeated measurements on two-component gradients of NPT/ClBMT in the same potential region (−0.5 to −1.2 V) reveal that the relative surface coverages change by <10%, indicating that little exchange occurs between NPT with ClBMT during the assembly of the second component. This observation agrees with previous contact angle measurements results on alkanethiol gradients.[8] Thus, by paying attention to the kinetics of exchange,

two-component gradients can be prepared with little perturbation to the original one-component system.

Two-component gradients of NPT/ACT were also formed, because these two thiols exhibit similar SERS enhancements. Unfortunately, the spectral separation is not as clean as it is for the NPT/ClBMT system. Nevertheless, it was possible to fit the spectral peaks and extract relative contributions from ACT and NPT. Changes in surface coverage of NPT after assembly of the second component, ACT, revealed the same behavior observed in NPT/ClBMT gradients. NPT coverage in the one-component film decayed to <5% of a full monolayer with a sigmoidal distribution across the film. When ACT was backfilled, the coverage of the second component also varied in a sigmoidal fashion in the opposite direction. The relative concentration of NPT did not change appreciably for any of the samples studied, but there was slightly more mixing and exchange at longer ACT assembly times.

Conclusions

Counterpropagating two-component gradients in surface composition are of interest in a number of applications. Electrochemical formation of these gradients allows the composition profiles to be shaped in both space and time, providing significant advantages over existing methods of gradient formation. Previous efforts to characterize the spatial characteristics of these gradients have relied on either physical methods, e.g., AFM or tagging reactions. In these experiments we demonstrate that surface-enhanced Raman spectroscopy is capable of providing functional group surface coverage maps of one- and two-component gradients of thiols containing aromatic pendant groups on thin Au films. When taken together, the requirements of in-plane electrical continuity and SERS activity severely constrains the range of substrates that can be employed. Thus, showing that MFON electrodes satisfy both requirements is significant. Characteristic vibrational modes of NPT and ClBMT were used to estimate surface coverage as a function of position (potential) on aromatic thiol-covered MFON electrodes to which gradients in electrochemical potential were applied. The resulting one-component gradients were characterized by a sigmoidal distribution in surface coverage as a function of position and potential along the film, thereby validating the linear potential approximation of eq 1 for these MFON electrodes. The thiol adsorbates were stable at positions corresponding to more positive potentials and were stripped at the negative end. Because the kinetics of reductive desorption of these aromatic thiols is relatively slow, longer electrolysis times (~30 min) were required to attain negative end coverages below 5% monolayer. SERS mapping of two-component gradients of both NPT/ClBMT and NPT/ACT was successful and revealed insignificant exchange (<10%) of the first component as long as the assembly time of the second component was kept relatively short (~1−2 min). Future efforts will focus on mapping functional group distributions in gradients of biologically active surface ligands involving protein adhesion promoters and inhibitors.

Acknowledgment. This work was supported by the National Science Foundation (CHE 99-10236) and by the Department of Energy (DE FG02 91ER45439). K.M.B. acknowledges the Electrochemical Society for providing an Edward G. Weston fellowship.

References and Notes

(1) Jeon, N. L.; Dertinger, S. K. W.; Chiu, D. T.; Choi, I. S.; Stroock, A. D.; Whitesides, G. M. *Langmuir* **2000**, *16*, 8311.

(2) Laibinis, P. E.; Nuzzo, R. G.; Whitesides, G. M. *J. Phys. Chem.* **1992**, *96*, 5097.

(3) Abbott, N. L.; Folkers, J. P.; Whitesides, G. M. *Science* **1992**, *257*, 1380.

(4) Bain, C. D.; Whitesides, G. M. *Science* **1988**, *240*, 62.

(5) Liedberg, B.; Tengvall, P. *Langmuir* **1995**, *11*, 3821.

(6) Fuierer, R. R.; Carroll, R. L.; Feldheim, D. L.; Gorman, C. B. *Adv. Mater.* **2002**, *14*, 154.

(7) Terrill, R. H.; Balss, K. M.; Zhang, Y.; Bohn, P. W. *J. Am. Chem. Soc.* **2000**, *122*, 988.

(8) Balss, K. M.; Coleman, B. D.; Lansford, C. H.; Haasch, R. T.; Bohn, P. W. *J. Phys. Chem. B* **2001**, *105*, 8970.

(9) Plummer, S. T.; Bohn, P. W. *Langmuir* **2002**, *18*, 4142.

(10) Balss, K. M.; Fried, G. A.; Bohn, P. W. *J. Electrochem. Soc.* **2002**, *149*, C450.

(11) Jayaraman, S.; Hillier, A. C. *Langmuir* **2001**, *17*, 7857.

(12) Schonherr, H.; Ringsdorf, H.; Jaschke, M.; Butt, H. J.; Bamburg, E.; Allinson, H.; Evans, S. D. *Langmuir* **1996**, *12*, 3898.

(13) Chechik, V.; Schonherr, H.; Vancso, G. J.; Stirling, C. J. M. *Langmuir* **1998**, *14*, 3003.

(14) Terrill, R. H.; Tanzer, T. A.; Bohn, P. W. *Langmuir* **1998**, *14*, 845.

(15) Zehner, R. W.; Sita, L. R. *Langmuir* **1997**, *13*, 2973.

(16) Dhirani, A. A.; Zehner, R. W.; Hsung, R. P.; Guyotsionnest, P.; Sita, L. R. *J. Am. Chem. Soc.* **1996**, *118*, 3319.

(17) Szafranski, C. A.; Tanner, W.; Laibinis, P. E.; Garrell, R. L. *Langmuir* **1998**, *14*, 3570.

(18) Sabatani, E.; Cohen-Boulakia, J.; Bruening, M.; Rubinstein, I. *Langmuir* **1993**, *9*, 2974.

(19) Tao, Y. T.; Wu, C. C.; Eu, J. Y.; Lin, W. L. *Langmuir* **1997**, *13*, 4018.

(20) Bandyopadhyay, K.; Vijayamohanan, K.; Venkataramanan, M.; Pradeep, T. *Langmuir* **1999**, *15*, 5314.

(21) Kolega, R. R.; Schlenoff, J. B. *Langmuir* **1998**, *14*, 5469.

(22) Szafranski, C. A.; Tanner, W.; Laibinis, P. E.; Garrell, R. L. *Langmuir* **1998**, *14*, 3580.

(23) Chang, S. C.; Chao, I.; Tao, Y. T. *J. Am. Chem. Soc.* **1994**, *116*, 6792.

(24) Yang, X. M.; Tryk, D. A.; Hashimoto, K.; Fujishima, A. *J. Raman Spectrosc.* **1998**, *29*, 725.

(25) Ye, Q.; Fang, J.; Sun, L. *J. Phys. Chem. B* **1997**, *101*, 8221.

(26) Young, J. T.; Boerio, F. J.; Zhang, Z.; Beck, T. L. *Langmuir* **1996**, *12*, 1219.

(27) Murty, K. V. G. K.; Venkataramanan, M.; Pradeep, T. *Langmuir* **1998**, *14*, 5446.

(28) Sanchez-Cortes, S.; Domingo, C.; Garcia-Ramos, J. V.; Aznarez, J. A. *Langmuir* **2001**, *17*, 1157.

(29) Olson, L. G.; Lo, Y. S.; Beebe, T. P.; Harris, J. M. *Anal. Chem.* **2001**, *73*, 4268.

(30) Grabar, K. C.; Allison, K. J.; Baker, B. E.; Bright, R. M.; Brown, K. R.; Griffith Freeman, R.; Fox, A. P.; Keating, C. D.; Musick, M. D.; Natan, M. J. *Langmuir* **1996**, *12*, 2353.

(31) Maxwell, D. J.; Emory, S. R.; Nie, S. M. *Chem. Mater.* **2001**, *13*, 1082.

(32) Kubo, S.; Gu, Z. Z.; Tryk, D. A.; Ohko, Y.; Sato, O.; Fujishima, A. *Langmuir* **2002**, *18*, 5043.

(33) Shen, A. J.; Pemberton, J. E. *J. Electroanal. Chem.* **1999**, *479*, 32.

(34) Schoenfisch, M. H.; Pemberton, J. E. *Langmuir* **1999**, *15*, 509.

(35) Schoenfisch, M. H.; Ross, A. M.; Pemberton, J. E. *Langmuir* **2000**, *16*, 2907.

(36) Brolo, A. G.; Irish, D. E.; Szymanski, G.; Lipkowski, J. *Langmuir* **1998**, *14*, 517.

(37) Dick, L. A.; McFarland, A. D.; Haynes, C. L.; Van Duyne, R. P. *J. Phys. Chem. B* **2002**, *106*, 853.

(38) Hatchett, D. W.; Uibel, R. H.; Stevenson, K. J.; Harris, J. M.; White, H. S. *J. Am. Chem. Soc.* **1998**, *120*, 1062.

(39) Hatchett, D. W.; Stevenson, K. J.; Lacy, W. B.; Harris, J. M.; White, H. S. *J. Am. Chem. Soc.* **1997**, *119*, 6596.

(40) Xiao, Y. J.; Markwell, J. P. *Langmuir* **1997**, *13*, 7068.

(41) Widrig, C. A.; Chung, C.; Porter, M. D. *J. Electroanal. Chem.* **1991**, *310*, 335.

(42) Sabatani, E.; Rubinstein, I. *J. Phys. Chem.* **1987**, *91*, 6663.

(43) Zhang, Y.; Terrill, R. H.; Bohn, P. W. *J. Am. Chem. Soc.* **1998**, *120*, 9969.

(44) Zhang, Y.; Terrill, R. H.; Bohn, P. W. *Anal. Chem.* **1999**, *71*, 119.

(45) Fried, G. A.; Zhang, Y.; Bohn, P. W. *Thin Solid Films* **2001**, *401*, 171.

(46) Based on molecular simulations with Cerius2 (Accelrys, Inc.) and Gaussian 98 (Gaussian Inc).